J Neurophysiol 112: 1838–1848, 2014.
First published July 16, 2014; doi:10.1152/jn.00909.2013.

Individual differences in intrinsic brain connectivity predict decision strategy

Kelly Anne Barnes, Kevin M. Anderson, Mark Plitt, and Alex Martin
Section on Cognitive Neuropsychology, Laboratory of Brain and Cognition, National Institute of Mental Health, National Institutes of Health, Bethesda, Maryland

Submitted 23 December 2013; accepted in final form 10 July 2014

Barnes KA, Anderson KM, Plitt M, Martin A. Individual differences in intrinsic brain connectivity predict decision strategy. *J Neurophysiol* 112: 1838–1848, 2014. First published July 16, 2014; doi:10.1152/jn.00909.2013.—When humans are provided with ample time to make a decision, individual differences in strategy emerge. Using an adaptation of a well-studied decision making paradigm, motion direction discrimination, we probed the neural basis of individual differences in strategy. We tested whether strategies emerged from moment-to-moment reconfiguration of functional brain networks involved in decision making with task-evoked functional MRI (fMRI) and whether intrinsic properties of functional brain networks, measured at rest with functional connectivity MRI (fcMRI), were associated with strategy use. We found that human participants reliably selected one of two strategies across 2 days of task performance, either continuously accumulating evidence or waiting for task difficulty to decrease. Individual differences in decision strategy were predicted both by the degree of task-evoked activation of decision-related brain regions and by the strength of pretask correlated spontaneous brain activity. These results suggest that spontaneous brain activity constrains strategy selection on perceptual decisions.

strategy; decision making; individual differences; fMRI; fcMRI

DECISIONS INVOLVE a set of core steps. Individuals process sensory signals, evaluate them for relevant evidence, and indicate decisions with motor responses (Gold and Shadlen 2007). However, with increased time available for a decision, variability in decision speed and strategy emerges. Consider two people seated at a diner, contemplating what to eat. One skims the menu and quickly decides on an order. The other shifts attention (e.g., between the menu and specials board) or pauses the decision process until more information can be obtained from the waiter. Cross-subject variability in decision strategy results partly from stable behavioral factors, including cognitive abilities (Aminoff et al. 2012; Badre et al. 2012; Bruine de Bruin et al. 2007; Meriau et al. 2006; Stanovich and West 2000), personality (Aminoff et al. 2012; Liverant and Scodel 1960; Soane and Chmiel 2005), and willingness to acquire costly evidence (Furl and Averbeck 2011; Treadway et al. 2009). Many studies examining the neural basis of decision making use quick, perceptual tasks to curtail variability in strategy. Therefore, little is known about neural mechanisms that account for cross-subject variability in decision strategy. Do stable strategies emerge from moment-to-moment reconfiguration of functional brain networks involved in decision making? Or do intrinsic network properties constrain the strategies to which individuals reliably turn?

Here we examined the neural basis of strategy differences during motion direction discrimination. This task provides a strong foundation for investigating strategy; the neurobiological circuitry underlying motion direction decisions is well established in nonhuman primates (Britten et al. 1992) and humans (Heekeren et al. 2006; Kayser et al. 2010). In our study, participants determined the direction of motion for noisy dot kinematograms. We manipulated stimulus coherence within trials, such that coherence doubled every 2 s in each 6-s trial (Fig. 1). We hypothesized that participants would use one of two strategies. People could continuously evaluate evidence, as in sequential sampling models (Ratcliff 1978), or, if they failed to reach a decision upon initial inspection, they could wait for a coherence increase before accumulating further evidence (henceforth "expedited" vs. "wait and see" accumulation strategies, respectively). Strategy was determined from the reaction time (RT) distribution across trials on 2 days of in-scanner task performance. Strategy, as quantified by this cumulative approach, is thus more closely aligned with concepts including "set characteristic" or "trait" behaviors than with behaviors influenced by situational factors.

We probed the neural basis of decision strategy with task-based functional MRI (fMRI) and resting-state functional connectivity MRI (fcMRI). Using fMRI, we quantified temporal characteristics of the task-evoked BOLD signal to determine the decision process stage (i.e., sensory processing, evidence accumulation, or decision/response selection) to which a brain region contributed (Ploran et al. 2007). The approach leverages response time-dependent or -independent changes in BOLD signal timing (i.e., onset, time to peak, and time course width), making the following assumptions: Sensory regions should become active when the stimulus is presented and remain active until the stimulus terminates; such regions should not show activity that varied with subjects' decision time. Regions that are involved in evidence accumulation would become active after sensory regions, and they would continue to be active until evidence reached a decision threshold. So, the onset point of these regions should not vary with decision time, but the time to peak should. Consequently, earlier responses would elicit narrower BOLD time courses than later responses. Regions involved in applying a decision rule would become active after evidence reaches a threshold. At this time, a response would be prepared and generated. So, for these regions, onsets and time to peak should vary with decision times; decision regions should also have the narrowest time courses, and time course width should not vary with decision time.

Strategy effects were anticipated in regions performing particular decision-related computations. We predicted that an "expedited" rather than "wait and see" accumulation strategy should yield stronger activation in regions identified as evidence accumulators. This prediction, which may

Address for reprint requests and other correspondence: K. A. Barnes, One Baylor Plaza, Rm. T115, MS: BCM295 Baylor College of Medicine, Houston, TX 77030 (e-mail: kelly.barnes@bcm.edu).

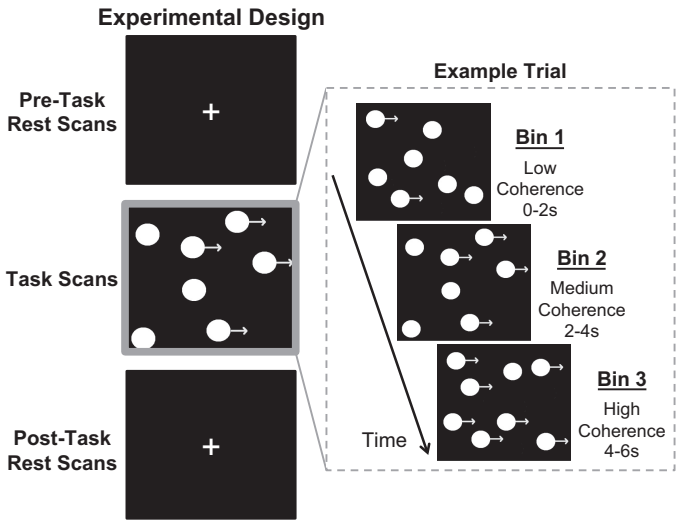

Fig. 1. Illustration of the experimental design and of the trial structure for a single example trial. On each trial, the percentage of coherently moving dots doubled every 2 s.

seem counterintuitive at first glance, stems from the following idea: if we look at decisions made at roughly the same time across subjects using different strategies, people who are continuously accumulating evidence, instead of pausing the decision process, should have greater activation in evidence accumulation regions. By extension, the difference between subjects using different strategies should increase with time spent accumulating evidence (i.e., for decisions made in later in the 6-s trial).

Using fcMRI, we examined coupling at rest between decision regions to determine whether intrinsic brain connectivity predicted strategy. Here we tested whether groups identified by their strategy differed in the strength of correlation between decision-related brain regions in the absence of, and prior to, task performance. Results indicated that intrinsic coupling between decision-related brain regions predicts decision strategy.

MATERIALS AND METHODS

Subjects

Twenty-six right-handed, native English-speaking adult participants with normal or corrected-to-normal vision were recruited from the National Institutes of Health. Participants were screened at the National Institute of Mental Health for current or past psychiatric or neurological conditions and were not taking any centrally acting medications. Informed consent was obtained from each participant in accordance with a protocol approved by the National Institutes of Health Institutional Review Board. Participants were compensated monetarily for participation.

Five participants were excluded from all analyses for chance task performance ($n = 3$), excessive head motion ($n = 1$), or inability to complete the second visit ($n = 1$). An additional three participants were excluded from the fMRI analyses for having an insufficient distribution of responses across response bins for analysis; however, these subjects were included in the fcMRI analyses. The fMRI analyses thus included 18 participants [10 men, 8 women; ages 21–25 yr (mean = 22.83 yr)], and the fcMRI analyses included 21 participants [10 men, 11 women; ages 20–26 yr (mean = 23.0 yr)].

Stimuli

Subjects viewed dot kinematograms of either plain circles or red dots in circles (Gao et al. 2010).[1] Stimuli were generated with Psychophysics Toolbox version 3 (Brainard 1997; Pelli 1997) in MATLAB (R2011a) and Variable Coherence Random Dot Motion Scripts (https://www.shadlenlab.columbia.edu/resources/VCRDM.html). Stimuli were generated with a dot size of 20 pixels and maximum dot density of 16.7 dots/frame. Dot density was set at 16.7 dots per square degree per second. Dot velocity was 5°/s. Motion coherence doubled every 2 s over a 6-s stimulus presentation, across two levels of increasing stimulus coherence (16% → 32% → 64% and 22% → 44% → 88%). Stimuli were front projected within a 1.80° square aperture.

Decision Making Paradigm

Participants viewed either plain circles or red dots in circles on separate days (order counterbalanced across subjects). Stimuli were presented as videos with Presentation software (NeuroBehavioral Systems). For each level of coherence, five different videos were generated so that the signal and noise varied on each trial. On each day, participants completed 196 trials, thus viewing each of the 5 unique stimulus videos ~39 times. For each trial, subjects were instructed to indicate the direction of motion (left/right) by button press with their left or right thumb, respectively, on an MRI-compatible button box (Current Designs). Subjects were instructed to respond as quickly and as accurately as possible. Stimuli were displayed for 6 s irrespective of response time to facilitate an analytic approach based on whether a region's response varied as a function of the subject's decision time. It was thus essential that the stimulus duration and response times be decoupled, although this limits the nature of the cognitive questions that can be asked with this task.

There was nothing tangible to be gained (i.e., no reward) for faster or more accurate responding. Furthermore, participants were aware that faster responses would not accelerate the completion of the task because they were informed of the fixed stimulus duration irrespective of response time. Therefore, there was no intrinsic reward associated with ending the trial for faster performance.

Image Acquisition

Data were acquired on a GE MR 750 3-T system using a GE 32-channel head coil. Structural images were acquired with a sagittal magnetization prepared rapid gradient echo (MP-RAGE) T1-weighted sequence [time echo (TE) = 3.42 ms; time repetition (TR) = 7 ms; time to inversion (TI) = 425 ms; flip angle = 7°; phase acceleration factor = 2; 176 slices with 1 × 1 × 1-mm voxels]. Functional images for task runs were obtained with an axial echo-planar imaging (EPI) sequence (TE = 27 ms; TR = 2,000 ms; flip angle = 77°; phase acceleration factor = 2; forty-three 3-mm-thick slices with 3 × 3-mm voxels). Functional images for rest runs were obtained with an axial EPI sequence (TE = 28.1 ms; TR = 2,500 ms; flip angle = 77°; phase acceleration factor = 2; forty-four 3-mm-thick slices with 2 × 2-mm voxels). One hundred fifty-four volumes were acquired for each task run, and one hundred thirty-four volumes were acquired for each rest run. Physiological variables of heart rate and respiration were recorded during task and rest scans with a pulse oximeter placed on the left index finger and a pneumatic belt positioned at the level of the diaphragm, respectively.

[1] The latter stimulus type was used for an orthogonal analysis examining the effects of low-level cues on perceptions of animacy in nonsocial tasks. For these stimuli, the position of the red dots in the white circles was irrelevant to the task at hand (i.e., the red dots were not predictive of the direction of motion).

fMRI Preprocessing

fMRI preprocessing was conducted separately for each subject with programs in AFNI (Cox 1996). The first four volumes of the time series for each run were discarded from analysis. Volumes were time shifted to correct for slice time acquisition differences. Anatomical data were aligned to the EPI data, and registered anatomical data were warped into a Talairach version of the MNI group brain standard space (TT_N27). EPI data were volume registered and warped into standard space in a single transformation. Each volume of each run was blurred with a 4-mm full-width half-maximum (FWHM) Gaussian kernel. EPI data were scaled so that each voxel time series had a mean of 100.

fcMRI Preprocessing

fcMRI preprocessing was conducted separately for each subject (Gotts et al. 2012; Jo et al. 2010). Specifically, resting-state fcMRI data were despiked and corrected for physiological motion effects (Glover et al. 2000), the first four volumes of the time series were then discarded, volumes were time shifted to correct for slice time acquisition differences, and all volumes were registered to the first volume of the first run. Segmented MP-RAGE volumes generated with FreeSurfer (Fischl et al. 2002) were aligned to the EPI data and were used to generate subject-specific white matter, ventricle, and draining vessel masks (Jo et al. 2010). For each voxel, the following nuisance regressors and their derivatives were created: an average ventricle time series, an average draining vessel time series, a local average white matter time series, 6 parameter estimates for head motion, and 13 regressors for respiration from RETROICOR and RTV. These nuisance signals were detrended prior to regression, and a 4th-order baseline detrending was applied to the regression model. The predicted time series of these nuisance variables was then subtracted from the voxelwise time series, yielding a residual time series. Each volume of each run from this residual was blurred with a 6-mm FWHM Gaussian kernel, data were rescaled to reflect percent signal change, and the two runs for each subject were concatenated. Finally, data were warped into a Talairach version of the MNI group brain standard space (TT_N27).

Data Analysis

Behavioral data analysis. Percentage of correct responses and median RTs for correct trials were computed for each subject and session.

fMRI analysis. First-level analyses consisted of individual general linear models (GLMs) that included a parameter for each of 10 time points after stimulus onset (so, times 0–18 s) for each of three conditions of interest: correct responses made in time 0–2,000 ms (*bin 1* responses), correct responses made in 2,001–4,000 ms (*bin 2* responses), correct responses made in 4,001–6,200 ms (*bin 3* responses), and error trials. We employed a simple error model, which compiled all error types into a single regressor, rather than creating separate regressors for error type (omission vs. commission) or error RT. While the cohort's average error rate was ~10%, there was substantial variability in error rates across subjects (min = 0%; max = 40%). However, the near-ceiling accuracy for the majority of subjects would have yielded very few trials for this analysis. Additional nuisance signals in the first-level regressions included motion parameters and drift parameters (modeled as a 3rd-order polynomial). Volumes with head motion exceeding 0.3 mm/TR were censored from the first-level GLM.

Second-level analyses consisted of a Response Bin (*1–3*) × Time Point ANOVA conducted on *day 1* data to identify regions of interest (ROIs) active, or modulated by decision time, during motion direction decision making. We identified the 50 strongest peaks of activation from main effect of Time Point and Response Bin × Time Point interaction from *day 1* data. If regions overlapped within 10 mm of one another, one of the overlapping regions was randomly eliminated. This procedure resulted in 75 unique ROIs. An additional 3 ROIs were eliminated for <10% likelihood of being in gray matter based on probabilistic cytoarchitecture maps in standard space (Eickhoff et al. 2007), resulting in a final set of 72 ROIs for analysis.

Functional classification of ROIs. ROIs from *day 1* were applied to *day 2* data to extract independent time courses for functional classification of ROIs. Onset time, time to peak, and time course width were determined for each subject and response bin at each ROI. We determined whether the region showed activation or deactivation: activation was defined as a maximal percent signal change from baseline greater than zero; deactivation was defined as a maximal percent signal change from baseline less than zero. For activation ROIs, the onset time was defined as the first TR at which activity significantly exceeded baseline in the first-level GLM and the peak was defined as the maximum of the time series. For deactivation ROIs, the onset time was defined as the first TR at which activity significantly fell below baseline in the first-level GLM and the peak was defined as the minimum of the time series. Thus linear interpolation was not used to calculate onset; rather, the significance of the *t*-statistic associated with each time point in the first-level GLM was assessed, with a statistical cutoff of $P < 0.05$. This approach had the advantage of allowing us to estimate onset points on a subject-by-subject basis to yield multiple assessments per ROI, thereby allowing a regionwise test of onset. To estimate time course width, we generated 1,000 points between each time point and performed a linear interpolation between each pair of consecutive time points (Ploran et al. 2007). This interpolation transformed the original 10-point time course into a series of 9,001 points. Time course width was defined as the FWHM of the time series around the peak.

We identified three types of information processing profiles putatively involved in perceptual decision making. Sensory processing ROIs were defined by significantly stronger correlations (i.e., difference in Fisher *r* to *z* transformed correlation coefficients $P < 0.05$) of time series across response bins than for temporally shifted versions of those time series across response bins. Evidence accumulation ROIs were defined by a significant difference in time to peak across bins, but not onset. Decision/response selection ROIs were defined by a significant difference in onset time and time to peak. While the criteria for evidence accumulation and decision/response selection ROIs were mutually exclusive, the criteria for sensory ROIs were not mutually exclusive with the other two classifications. In the event that an ROI met criteria for two classifications (e.g., an ROI showed a small but statistically significant effect of response bins on either time to peak or onset and time to peak, but the time courses were generally more similar across response bins), we opted for the more conservative classification (i.e., sensory processing) but note all classifications an ROI met in Table 1.

fcMRI Analysis

For each ROI, time series were extracted for each subject and session and correlated, resulting in a 72 × 72 ROI matrix of correlations. Time points corresponding to periods of head motion > 0.3 mm/TR and time points two prior to and two subsequent to the flagged volumes were excluded from the correlation calculation, i.e., the data were motion scrubbed (Power et al. 2012). Scrubbed correlation coefficients were Fisher transformed to z' values to stabilize variance across the range of Pearson's *r* values.

RESULTS

Behavioral Results

Overall, decisions were highly accurate (*day 1*: mean = 91.01%, SD = 10.03; *day 2*: mean = 90.07%, SD = 11.57).

Table 1. *Complete listing of ROIs identified from the decision task*

X	*Y*	*Z*	Index	Anatomical Landmark	BA	Classification	Dir
−5	2	48	*1*	Presupplementary motor	6	—	Pos
11	−14	−1	*19*	Thalamus		—	Pos
56	−44	30	*23*	Supramarginal gyrus	40	—	Pos
−50	5	12	*24*	Precentral gyrus	44/6	—	Pos
−47	−26	21	*26*	Posterior insula		—	Pos
47	35	24	*28*	Middle frontal gyrus	46	—	Pos
35	−26	45	*29*	Postcentral gyrus	3	—	Pos
−35	−26	48	*32*	Precentral gyrus	3	—	Pos
53	−26	45	*33*	Postcentral gyrus	2	—	Pos
−35	−20	57	*37*	Precentral gyrus	4	—	Pos
−38	−53	−40	*39*	Cerebellum		—	Pos
29	−74	27	*45*	Cuneus	19	—	Pos
−44	5	30	*52*	Inferior frontal gyrus	9	—	Pos
−14	−23	15	*61*	Thalamus		—	Pos
−53	26	12	*62*	Inferior frontal gyrus	45	—	Pos
−56	−20	45	*63*	Postcentral gyrus	2	—	Pos
2	−23	30	*25*	Mid-cingulate gyrus	23	—	Neg
8	17	36	*4*	Anterior cingulate cortex	32	Accumulator	Pos
41	11	9	*5*	Anterior insula		Accumulator	Pos
8	−17	12	*6*	Thalamus		Accumulator	Pos
47	14	−1	*9*	Anterior insula/inferior frontal gyrus	47	Accumulator	Pos
32	44	27	*11*	Middle frontal gyrus	9	Accumulator	Pos
8	26	30	*12*	Anterior cingulate cortex	32	Accumulator	Pos
2	−77	−16	*21*	Cerebellum		Accumulator	Pos
41	41	18	*22*	Middle frontal gyrus	10	Accumulator	Pos
5	−62	−10	*27*	Cerebellum		Accumulator	Pos
−38	−5	18	*35*	Mid-insula		Accumulator	Pos
−26	−11	51	*44*	Precentral gyrus	6	Accumulator	Pos
32	−50	−25	*49*	Cerebellum		Accumulator	Pos
−32	−44	39	*51*	Intraparietal sulcus	40	Accumulator	Pos
−23	−65	48	*56*	Superior parietal lobule	7	Accumulator	Pos
11	−68	−40	*59*	Cerebellum		Accumulator	Pos
53	−20	27	*65*	Postcentral gyrus/inferior parietal lobule	2/40	Accumulator	Pos
−26	−74	27	*68*	Precuneus	31	Accumulator	Pos
2	−32	24	*18*	Posterior cingulate cortex	23	Accumulator	Neg
−41	−71	27	*64*	Angular gyrus	39	Accumulator	Neg
−29	23	9	*2*	Anterior insula		Decision	Pos
8	8	45	*3*	Presupplementary motor	6	Decision	Pos
−11	20	30	*7*	Anterior cingulate cortex	32	Decision	Pos
41	2	42	*10*	Middle frontal gyrus	6	Decision	Pos
8	−5	57	*13*	Supplementary motor area	6	Decision	Pos
−8	−11	51	*14*	Supplementary motor area	6	Decision	Pos
−56	−20	24	*15*	Supramarginal gyrus	40	Decision	Pos
−44	14	3	*17*	Insula/frontal operculum		Decision	Pos
−14	−8	21	*30*	Caudate		Decision	Pos
−11	−5	63	*31*	Superior frontal gyrus	6	Decision	Pos
14	−5	21	*36*	Caudate		Decision	Pos
−32	47	27	*38*	Superior frontal gyrus	9	Decision	Pos
44	2	27	*42*	Precentral gyrus/inferior frontal	9/6	Decision	Pos
32	26	9	*46*	Inferior frontal gyrus/insula	45/13	Decision	Pos
−32	−47	−25	*48*	Cerebellum		Decision	Pos
29	−47	42	*54*	Inferior parietal lobule	40	Decision	Pos
−47	−32	39	*55*	Inferior parietal lobule	40	Decision	Pos
5	−29	−1	*57*	Thalamus		Decision	Pos
41	−5	51	*58*	Precentral gyrus	6	Decision	Pos
32	−14	−4	*70*	Putamen		Decision	Pos
20	−62	−40	*72*	Cerebellum		Decision	Pos
8	−53	15	*67*	Posterior cingulate cortex	30	Decision	Neg
47	−77	−4	*41*	Inferior occipital gyrus	19	Sensory	Pos
−14	−89	15	*47*	Middle occipital gyrus	18	Sensory	Neg
−8	−74	−7	*50*	Lingual gyrus	18	Sensory	Neg
14	−86	3	*53*	Lingual Gyrus	17	Sensory	Neg
14	−80	21	*69*	Cuneus	18	Sensory	Neg
8	50	3	*71*	Ventromedial prefrontal cortex		Sensory	Neg
32	−89	6	*16*	Middle occipital gyrus	18	Sensory/accumulator	Pos
29	−83	−4	*8*	Inferior occipital gyrus	18	Sensory/decision	Pos
26	−92	−10	*20*	Inferior occipital gyrus/fusiform	18	Sensory/decision	Pos
−26	−92	−4	*34*	Inferior occipital gyrus	18	Sensory/decision	Pos

Continued

Table 1.—*Continued*

X	*Y*	*Z*	Index	Anatomical Landmark	BA	Classification	Dir
−32	−80	−7	*40*	Middle occipital gyrus	18	Sensory/decision	Pos
41	−62	−10	*43*	Fusiform gyrus	37	Sensory/decision	Pos
−23	−83	−19	*60*	Cuneus	18	Sensory/decision	Pos
−32	−74	−19	*66*	Fusiform gyrus	19	Sensory/decision	Pos

Coordinates (*X*, *Y*, *Z*) are reported in Talairach space with the nearest associated anatomical landmark. Index allows for cross-reference with Tables 2 and 3. BA denotes nearest Brodmann area. Classification denotes whether the region of interest (ROI) met criteria for 1 or more stage of the decision process; —, not classified. Direction (Dir) denotes whether the region showed a positive-going (Pos) or negative-going (Neg) BOLD signal change relative to baseline.

Median RT occurred approximately midway through the 6-s trial (*day 1*: mean = 2.62 s, SD = 0.80; *day 2*: mean = 2.59 s, SD = 1.05). Neither accuracy ($P = 0.88$) nor median RT ($P = 0.83$) differed across days, confirming that behavior was highly consistent across days (Fig. 2, *A* and *B*). Across individuals, however, median decision times (min = 0.87 s; max = 4.54 s) and RT distribution shape (Fig. 2*C*) varied widely. This variability in response speed and distribution suggested that participants might have employed different decision making strategies.

Decision strategy was determined from individuals' distribution of RTs across trials on both days of the task. "Expedited" evidence accumulation was expected to yield faster decisions and unimodal, positively skewed RT distributions [the hallmark RT distribution across a range of decision tasks (Balota and Yap 2011; Luce 1986; Ratcliff and McKoon 2008)]. For the "wait and see" strategy, we expected slower decisions and multimodal RT distributions, with troughs in the response time distributions corresponding to periods of increasing coherence. This pattern of results was expected to emerge if participants delayed the decision process until a pending coherence increase.

We quantified strategy by first determining the cumulative distribution function (CDF) for each subject's correct RTs. We then used this CDF to calculate two metrics at two time points: *1*) the proportion of responses that were executed by the time of the coherence increases (i.e., at 2 s and 4 s) and *2*) the differences in CDF values spanning the coherence increases (i.e., 2.25 s–1.75 s and 4.25 s–3.75 s). This approach was used to account for overall response speed (higher CDF values at 2 and 4 s would indicate faster responses because more responses would have been executed at the sampled times) and likelihood of responding around coherence increases (higher differences in CDF values around the coherence increases would indicate

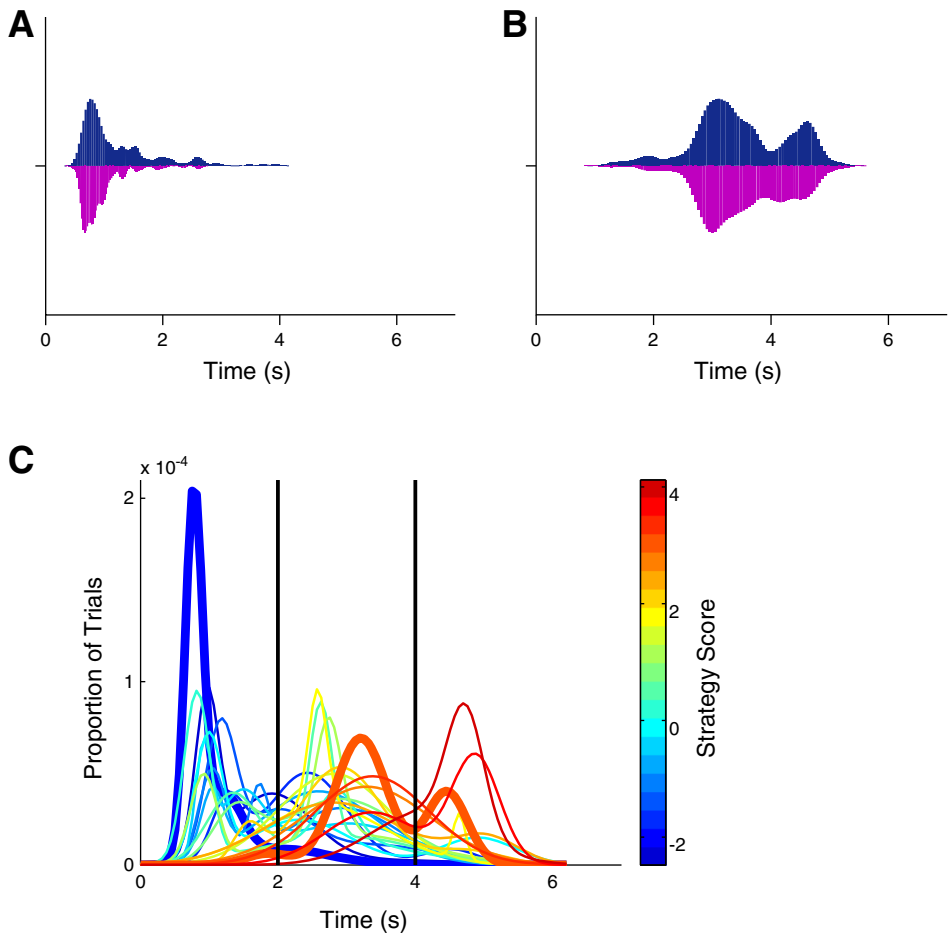

Fig. 2. *A* and *B*: histograms depicting distribution of response times for 2 example subjects, with data from *day 1* in blue and data from *day 2* in magenta. Histograms are normalized to facilitate comparison of distribution shapes across subjects. *C*: motion direction discrimination performance was variable across participants. Individual's fitted reaction time (RT) distributions are plotted as probability density functions by time. Line color depicts strategy score values determined from principal component analysis. Increases in stimulus coherence are marked by the vertical black lines at 2 s and 4 s. "Expedited" subjects were more likely to show a positively skewed, unimodal response distribution (example "expedited" subject's RT distribution, also shown in *A*, bold blue line), whereas slow subjects were more likely to show multimodal RT distributions (example "wait and see" subject's RT distribution, also shown in *B*, bold orange line).

a continuation of responses during coherence increases, while lower values would indicate a lack of responding during coherence increases, as would be expected if a subject employed the "wait and see" strategy and did not execute responses during a coherence increase).

A significant degree of correlation was expected between the CDF-based metrics because CDF values from earlier time points necessarily constrain CDF values at later time points. Thus principal component analysis was used to generate a set of uncorrelated components based on the four values calculated as described above. The first component explained 73.84% of the variance. The second component explained 17.18% of the variance but had an eigenvalue < 1. We therefore defined strategy as the weighted scores associated with the first principal component.

To validate and interpret our measure of strategy, we compared it to two metrics: median RT and model fits. As expected given its construction, strategy was significantly correlated with mean RT ($r = 0.93$, $P < 0.0001$). Strategy was also significantly correlated with the number of Gaussians comprising the model that best fit the RT distribution, comparing unimodal, bimodal, and trimodal distributions (Spearman's $\rho = -0.57$, $P = 0.007$), although the direction of this effect is opposite to our expectations as a consequence of the highly positively skewed data from the fastest subjects being better fit by trimodal than unimodal Gaussian functions (see Freeman and Dale 2013 for discussion). The behavioral data thus suggested a difference in decision making strategies across subjects, with some subjects rapidly and continuously accumulating evidence and other subjects sporadically accumulating evidence, waiting for intervals of increased stimulus coherence. These behavioral tendencies are reflected in subjects' strategy scores, where lower scores reflect a greater reliance on the "expedited" strategy and higher scores reflect a greater reliance on the "wait and see" strategy (Fig. 2*C*).

Identifying Brain Regions Involved in Decision Making

To determine the locations of brain regions involved in motion direction decisions, we identified the strongest peaks of activation from the first scan day (*day 1*) for two contrasts: *1*) significant activation changes in the BOLD signal during motion direction decisions (main effect of Time Point) or *2*) significant response time-dependent BOLD signal changes during decision making (Response Bin × Time Point interaction). Response bin was defined as the interval in which the response was made (*bin 1* = 0–2 s, *bin 2* = 2–4 s, *bin 3* = 4–6 s). All tests were conducted with a statistical cutoff of $P < 0.05$, FDR corrected. We identified the 50 strongest peaks of activation from main effect of Time Point and Response Bin × Time Point interaction analyses from *day 1* data. Regions within 10 mm of other another or with <10% likelihood of being in gray matter were eliminated, yielding a final set of 72 brain region ROIs. These ROIs included regions near established nodes of motion direction discrimination circuitry such as area MT+ and the intraparietal sulcus (IPS) (Fig. 3). A full listing of identified ROIs and their associated statistics appears in Table 1.

Classifying Information Processing in Identified Regions

To independently characterize functional processing, we analyzed the time course data from the second of the two scan sessions (*day 2*) by applying the ROIs identified on *day 1* to the *day 2* data. We classified brain regions on the basis of their temporal properties as involved in sensory processing, evidence accumulation, or decision/response selection. ROIs that failed to meet these statistical criteria were not assigned a classification. Our approach was unbiased regarding the direction of BOLD signal changes relative to baseline. Only positive-going regions involved in decision making are discussed here, excepting cases where strategy differences emerged involving regions with negative-going time courses.

Time course analysis identified 48 positive-going ROIs that met classification criteria: 10 sensory processing regions, 17 evidence accumulation regions, and 21 decision/response selection regions (see Table 1). Sensory processing ROIs were located in occipital and posterior temporal cortex, regions anticipated to be strongly engaged by visual motion (shown in red in Fig. 3). Accumulator ROI locations included the IPS, lateral frontal cortex, anterior cingulate cortex, and the cerebellum (shown in blue in Fig. 3). These results converge with neurophysiology studies in nonhuman primates that have identified neuronal firing patterns indicative of evidence accumulation in regions of the IPS and FEF. Decision/response selection ROIs were located in the anterior insula, presupplementary motor area, premotor cortex, anterior IPS, as well as subcortical and cerebellar structures (shown in green in Fig. 3). Decision/response selection signals were expected to emerge in motor regions, given that decisions were indicated via button press. In addition, these results converge with human imaging studies that have implicated the anterior insula and presupplementary motor cortex in decision selection (Kayser et al. 2010; Nelson et al. 2010; Ploran et al. 2007).

Strategy Differences in Task-Based fMRI Activation

We then tested whether any of the ROIs identified on *day 1* showed significant differences in activation strength on *day 2* as a function of participants' strategy scores ($P < 0.05$, Bonferroni corrected for multiple comparisons across the 3 levels of Response Bin). Specifically, we tested for a correlation between BOLD signal change at the peak time point in each ROI's time course and strategy scores for each response bin. Two patterns of group differences emerged (Table 2 and Fig. 4*A*). First, a positive correlation between strategy score and magnitude of activation was seen in two occipital ROIs that met criteria for sensory processing. These results indicated that subjects using a "wait and see" strategy were more likely to recruit regions involved in early, sensory stages of the decision process.

Second, a negative correlation was seen between strategy scores and magnitude of activation in 17 ROIs, 6 of which met criteria for evidence accumulation, 6 of which met criteria for decision/response selection, and 5 of which were unclassified. Negative correlations here indicated a stronger degree of activation in subjects using the "expedited" strategy rather than the "wait and see" strategy. These regions were located in the anterior insula bilaterally, anterior cingulate cortex, posterior parietal cortex, lateral prefrontal cortex, and subcortical structures. These results are consistent with our prediction that an

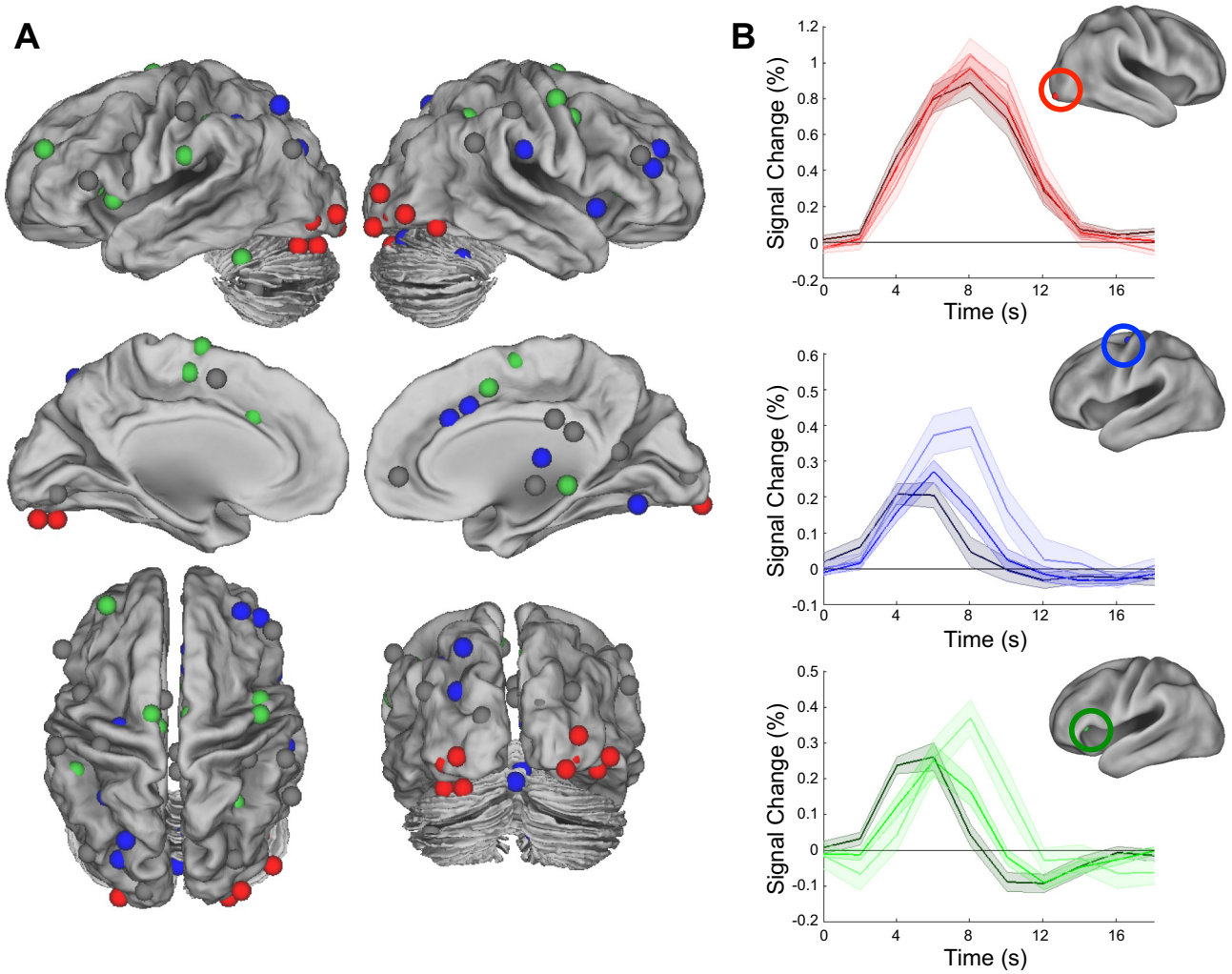

Fig. 3. *A*: locations of regions of interest (ROIs) meeting criteria for sensory processing (red), evidence accumulation (blue), and decision/response selection (green). Unclassified regions are shown in gray. *B*: time courses for an example sensory region in inferior occipital gyrus [29, −83, −4; *top*], an evidence accumulation region in premotor cortex [−26, −11, 51; *middle*], and a decision/response selection region in the anterior insula [−29, 23, 9; *bottom*] reveal regional variability in BOLD signal onset time, time to peak, and full width at half maximum as a function of decision time. Time courses from *bins 1–3* are shown from darkest to lightest shades. *Inset* brains in *B* depict location of ROI on an inflated surface.

"expedited" rather than a "wait and see" strategy would yield greater activation in evidence accumulation regions. Compared with the sensory regions that showed a positive correlation with strategy score, these results indicated that subjects using an "expedited" accumulation strategy were more likely to recruit regions involved in later stages of the decision process (evidence accumulation and decision/response selection).

Strategy Differences in Resting-State fcMRI Correlation Strength

All participants underwent resting-state scanning before and after their task scans on both days (Fig. 1). We examined these resting-state data to determine whether group differences in decision strategy were related to intrinsic brain connectivity. To focus our analysis on decision-related circuitry, we applied the 72 ROIs identified in the task-based fMRI analysis to the resting-state data and computed the correlation coefficients between these brain regions at rest.

The pretask data from the first day of scanning (*rest session 1*) was reserved for our key test: whether resting-state functional connectivity strength predicted decision strategy. The remaining data (i.e., ROI to ROI correlation values from *rest sessions 2–4*) were used for feature selection. This two-step approach was employed to reduce the dimensionality of a large, 72 × 72 connection matrix, thereby minimizing the potential for statistical overfitting. We used multivariate machine learning regression methods (support vector regression and ridge regression) to determine the degree to which resting-state fcMRI data predicted decision strategy.

Feature selection results. This analysis was conducted with resting-state data from all sessions except the pretask scans on *day 1* to identify candidate connections that might be strong predictors of subsequent decision strategy. We identified connections that reliably correlated with participants' strategy scores across sessions acquired after task performance [*day 1* post task ($P < 0.1$) × *day 2* pre task ($P < 0.1$) × *day 2* post task ($P < 0.1$), yielding a combined probability of $P < 0.001$]. Group differences in correlation strength were seen in 12 connections (Table 3), showing three main patterns of differences. First, strategy scores positively correlated with fcMRI

Table 2. *Regions of interest where fMRI activation significantly correlated with strategy scores*

X	*Y*	*Z*	Anatomical Landmark [index; response bin(s)]	Classification
Positive correlation with strategy score (greater in "wait and see")				
−26	−92	−4	Inferior occipital gyrus (*34*; *1*)	Sensory
−32	−80	−7	Middle occipital gyrus (*40*; *1*)	Sensory
Negative correlation with strategy score (greater in "expedited")				
47	35	24	Middle frontal gyrus (*28*; *2*)	—
−44	5	30	Inferior frontal gyrus (*52*; *3*)	—
−35	−20	57	Precentral gyrus (*37*; *2*)	—
11	−14	−1	Thalamus (*19*; *2*)	—
−14	−23	15	Thalamus (*61*; *2*)	—
8	26	30	Anterior cingulate cortex (*12*; *2,3*)	Accumulator
32	44	27	Middle frontal gyrus (*11*; *2*)	Accumulator
5	−62	−10	Cerebellum (*27*; *2*)	Accumulator
8	−17	12	Thalamus (*6*; *2*)	Accumulator
8	17	36	Anterior cingulate cortex (*4*; *2*)	Accumulator
−23	−65	48	Superior parietal lobule (*56*; *3*)	Accumulator
−44	14	3	Insula/frontal operculum (*17*; *3*)	Decision
41	−5	51	Precentral gyrus (*58*; *2*)	Decision
−56	−20	24	Supramarginal gyrus (*15*; *1*)	Decision
41	2	42	Middle frontal gyrus (*10*; *2,3*)	Decision
14	−5	21	Caudate (*36*; *2*)	Decision
5	−29	−1	Thalamus (*57*; *2*)	Decision

Coordinates (*X*, *Y*, *Z*) are reported in Talairach space with the nearest associated anatomical landmark and associated index number and response bin. Full ROI details appear in Table 1 by index number. Classification denotes whether the ROI met criteria for 1 or more stage of the decision process; —, not classified. fMRI, functional MRI.

strength for four connections, including two connections to an occipital sensory region that deactivated during the task. Second, strategy scores negatively correlated with frontal and parietal brain regions involved in evidence accumulation and other frontal brain regions. Third, strategy scores negatively correlated with anterior insula regions involved in decision/response selection.

Eight of the twelve connections that showed strategy differences in resting-state correlation strength also showed strategy differences in task-evoked activation (see Table 3). Given our thresholds for the tests of group differences ($P < 0.0167$ for the fMRI/task data and a combined probability of $P < 0.0001$ for the rest data), 1 out of 72 regions would be expected to show a group difference in task and rest due to chance. The observed overlap in 8 of 72 regions far exceeds chance levels, suggesting that intrinsic differences in neural circuitry may have given rise to individual differences in decision speed and strategy.

Regression results. We examined the first day's pretask resting-state data to determine the degree to which strategy was predicted by functional connectivity. This analysis allows us to rule out the possibility that the strategy differences in resting-state data were solely driven by the posttask scans. We used the 12 connections identified in the feature selection step in this analysis. Across two machine learning regression methods, pretask resting-state fcMRI data explained a statistically significant amount of variance in subsequent decision strategy (ridge regression $r^2 = 0.315$, $P = 0.001$; support vector regression $r^2 = 0.179$, $P = 0.025$). (We also report the univariate correlation between strategy score and pretask *day 1* resting-state data in Table 3). Collectively, these data suggest that individual differences in intrinsic brain connectivity predict decision strategy, with a medium to large effect size. The mean feature weights from the ridge regression analysis (averaged across cross-validation folds) are depicted in Fig. 4*B*. Mean feature weights from the ridge regression analysis were highly correlated with mean feature weights in the support vector regression analysis ($r = 0.96$).

DISCUSSION

Intrinsic brain connectivity reliably predicted stable individual decision strategy. These findings provide a neural basis for the long-standing observation that consistent aspects of individuals' personalities and abilities constrain decision strategy (Aminoff et al. 2012; Badre et al. 2012; Bruine de Bruin et al. 2007; Furl and Averbeck 2011; Liverant and Scodel 1960; Meriau et al. 2006; Soane and Chmiel 2005; Stanovich and West 2000; Treadway et al. 2009). In our study, participants

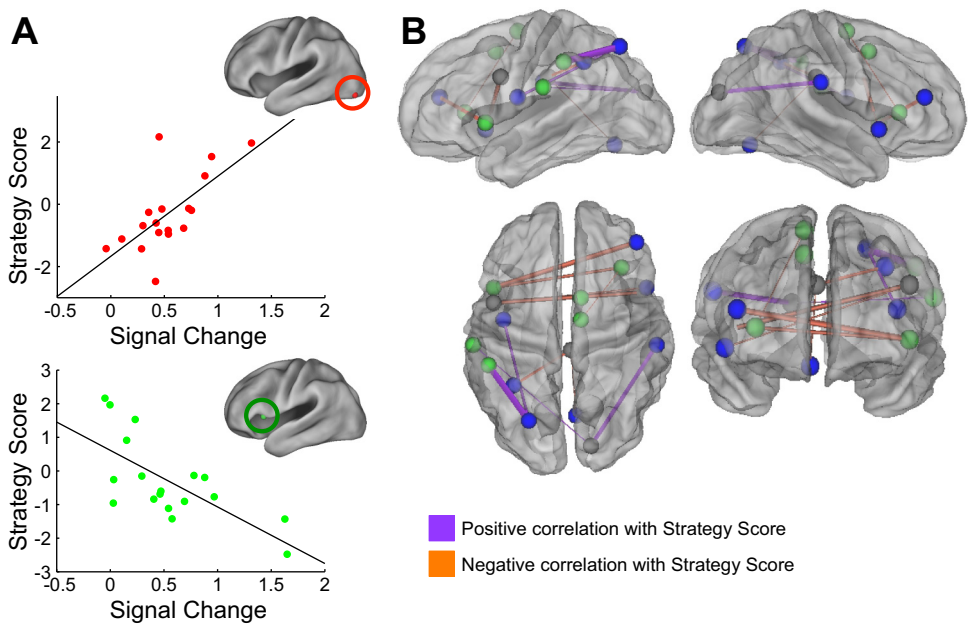

Fig. 4. *A*: regions showing strategy differences in task-evoked activation. *Top*: a sensory region in inferior occipital gyrus [−32, −80, −7]. *Bottom*: a decision region in the anterior insula [−44, 14, 3]. *B*: feature weights associated with strategy differences at rest; stronger connections in "expedited" subjects are shown in orange, and stronger connections in "wait and see" subjects are shown in purple. Spheres depict the classification of ROIs with conventions from Fig. 3.

Table 3. *Connections showing significant functional connectivity strength by strategy score correlations*

X, Y, Z	Anatomical Landmark (index)	Classification	*X, Y, Z*	Anatomical Landmark (index)	Classification	Mean Connectivity	fMRI Strategy Effect	Mean Posttask fcMRI × Strategy	*Day 1* Pretask × Strategy
Positive correlation between functional connectivity strength and strategy score (greater in "wait and see")									
14, −80, 21	Cuneus (*69*)	Sensory	53, −20,27	Postcentral gyrus/inferior parietal lobule (*65*)	Accumulator	0.22	No	0.51	0.49
14, −80, 21	Cuneus (*69*)	Sensory	−56, −20,24	Supramarginal gyrus (*15*)	Decision	0.22	Yes	0.40	0.20
−23, −65, 48	Superior parietal lobule (*56*)	Accumulator	−38, −5,18	Mid-insula (*35*)	Accumulator	0.21	Yes	0.43	0.37
−23, −65, 48	Superior parietal lobule (*56*)	Accumulator	−47, −32,39	Inferior parietal lobule (*55*)	Decision	0.44	Yes	0.43	0.56
Negative correlation between functional connectivity strength and strategy score (greater in "expedited")									
5, −62, −10	Cerebellum (*27*)	Accumulator	2, −23,30	Mid-cingulate gyrus (*25*)	—	0.08	Yes	−0.45	−0.20
−32, −44, 39	Intraparietal sulcus (*51*)	Accumulator	2, −23,30	Mid-cingulate gyrus (*25*)	—	0.01	No	−0.44	−0.31
41, 11, 9	Anterior insula (*5*)	Accumulator	−44, 5,30	Inferior frontal gyrus (*52*)	—	0.17	Yes	−0.48	−0.43
47, 14, −1	Anterior insula/inferior frontal gyrus (*9*)	Accumulator	−44, 5,30	Inferior frontal gyrus (*52*)	—	0.17	Yes	−0.39	−0.23
41, 41, 18	Middle frontal gyrus (*22*)	Accumulator	−44, 14, 3	Insula/frontal operculum (*17*)	Decision	0.26	Yes	−0.56	−0.50
8, 8, 45	Presupplementary motor cortex (*3*)	Decision	2, −23,30	Mid-cingulate gyrus (*25*)	—	0.12	No	−0.52	−0.33
−44, 14, 3	Insula/frontal operculum (*17*)	Decision	32, 26, 9	Inferior frontal gyrus/insula (*46*)	Decision	0.38	Yes	−0.53	−0.31
8, −5, 57	Supplementary motor area (*13*)	Decision	32, 26, 9	Inferior frontal gyrus/insula (*46*)	Decision	0.25	No	−0.39	−0.28

Conventions as in Table 2. Classification denotes whether the ROI met criteria for 1 or more stage of the decision process; —, not classified. "Mean connectivity" reports the average ROI-ROI correlation across all subjects and sessions. "fMRI strategy effect" denotes whether a ROI in that pair also shows a significant correlation between task-evoked activation and strategy scores. "Mean posttask fcMRI × strategy" reports the average *r* value across 3 strategy score correlation tests. "Day 1 Pretask × strategy" reports the correlation between functional connectivity strength and strategy scores for the pretask resting-state session. fcMRI, functional connectivity MRI.

varied in the strategy they used to perform a motion direction discrimination paradigm. Across 2 days, participants either expeditiously accumulated evidence or paused the decision process intermittently, waiting for the task difficulty to decrease before reinitiating the decision process ("expedited" vs. "wait and see" accumulation strategy). We employed a data-driven approach to classify information processing in decision-related brain regions. The results supported our key prediction: subjects relying more heavily on the "expedited" accumulation strategy showed stronger task-evoked activation of, and stronger resting-state correlations between, regions that performed evidence accumulation. The pretask resting-state data also allowed us to identify connections that differed in strength before task performance, providing evidence that intrinsic connectivity predicted strategy.

Stronger coupling of brain regions that performed evidence accumulation biased participants toward the use of the more efficient, "expedited" strategy that yielded faster decision times. The extended stimulus reveal in the present paradigm places high demands on mechanisms of evidence accumulation, as participants must integrate noisy perceptual information over a long time window (up to several seconds instead of several hundred milliseconds as in most typical perceptual decision making paradigms). Thus evidence accumulation in the present paradigm may place high demands on sustained attention. Two of the prefrontal brain regions that show connectivity-behavior relationships in the present study, the anterior insula and the anterior cingulate cortex, are among the most consistent locations of brain activation across a range of attention-demanding cognitive tasks (Duncan and Owen 2000; Nelson et al. 2010). The robust recruitment of these regions suggests that they may contribute to a general-purpose process. Indeed, the anterior insula and anterior cingulate comprise a core control network that makes particular contributions to sustained attention and task set (Dosenbach et al. 2008). We reference these meta-analytic studies to leverage a forward inference with regard to possible functional roles for these loci of group differences. In any event, it would be difficult to discern whether greater activation in these regions by the "expedited" subjects reflects exclusively greater decision-related activity or instead some combination of greater decision and nondecision processing that might be colocalized within the same voxels. Eye tracking may be a powerful complementary tool for disentangling the effects of decision and nondecision processes such as attention and task set (e.g., Krishna et al. 2014). Interestingly, these anterior insula and anterior cingulate regions have also shown connectivity-behavior relationships during shape identification tasks (Baldassarre et al. 2012) and cognitive control measured with the flanker task (Mennes et al. 2011), consistent with a more general-purpose role for this circuitry. Future studies could directly test the idea that sustained attention mediates the relationship between decision strategy and connectivity with insula and cingulate regions that perform evidence accumulation.

One unexpected result was the finding of stronger activation of sensory brain regions in participants who used a "wait and see" strategy. One possibility is that the greater activation of sensory regions reflects a "time on task" effect, despite the fact that strategy effects were seen when matching roughly for RT with the binwise analysis. This speculation is supported by the lack of overlap between these regional activation differences and regions showing group differences in connectivity at rest, when time on task is not a confounding factor. On a related point about behavior, our behavioral measure of strategy was

defined from each participant's distribution of responses across 2 days of task performance. Overall accuracy was high (~90%), and accuracy did not correlate significantly with strategy ($r = -0.13$, $P = 0.57$), so it is unlikely that any trade-offs between strategy/speed and accuracy were at play in the present version of the task. This lack of a speed-accuracy trade-off is less surprising in light of our task, which involved a relatively protracted 6-s interval over which subjects could make their decision.

Finally, it is noteworthy that there was substantial overlap in the brain regions that showed strategy differences at rest and in task-evoked activation. [Two-thirds of the connections (8/12) that showed strategy differences in resting-state correlation strength also showed strategy differences in task-evoked activation.] This observation is consistent with recent studies reporting overlap in resting-state and task-evoked individual differences associated with shape identification (Lewis et al. 2009) and cognitive control (Mennes et al. 2010). Recent work has shown that resting-state fcMRI signal fluctuations are strongly correlated with neuronal firing patterns, having been linked to slow cortical potentials (He et al. 2008) and band-limited power in the gamma frequency (Leopold and Maier 2012). In addition, regions displaying strong fcMRI correlation strength largely, but not entirely, overlap with monosynaptically connected brain regions and are related to anatomical connection strength indexed with diffusion tensor imaging (Honey et al. 2009). Thus group differences in fcMRI strength may reflect subtle differences in correlated neuronal firing or anatomical connection strength. Although exactly how slow fluctuations in the fMRI signal relate to or modulate task-evoked responses is not fully understood, the present study strongly suggests that intrinsic connection strength can predispose or constrain the set of strategies that individuals employ when faced with a decision.

ACKNOWLEDGMENTS

We thank Vinny Costa, Steve Gotts, and Jeff Yau for helpful discussion and Gang Chen, Steve Gotts, and Hang Joon Jo for technical assistance.

GRANTS

This work was supported by the National Institute of Mental Health, Division of Intramural Research Programs, project number ZIA MH-002588-23.

DISCLOSURES

No conflicts of interest, financial or otherwise, are declared by the author(s).

AUTHOR CONTRIBUTIONS

Author contributions: K.A.B., M.P., and A.M. conception and design of research; K.A.B. and K.M.A. performed experiments; K.A.B., K.M.A., and M.P. analyzed data; K.A.B., K.M.A., M.P., and A.M. interpreted results of experiments; K.A.B. and K.M.A. prepared figures; K.A.B. drafted manuscript; K.A.B., K.M.A., M.P., and A.M. edited and revised manuscript; K.A.B., K.M.A., M.P., and A.M. approved final version of manuscript.

REFERENCES

Aminoff EM, Clewett D, Freeman S, Frithsen A, Tipper C, Johnson A, Grafton ST, Miller MB. Individual differences in shifting decision criterion: a recognition memory study. *Mem Cognit* 40: 1016–1030, 2012.

Badre D, Doll BB, Long NM, Frank MJ. Rostrolateral prefrontal cortex and individual differences in uncertainty-driven exploration. *Neuron* 73: 595–607, 2012.

Baldassarre A, Lewis CM, Committeri G, Snyder AZ, Romani GL, Corbetta M. Individual variability in functional connectivity predicts performance of a perceptual task. *Proc Natl Acad Sci USA* 109: 3516–3521, 2012.

Balota DA, Yap MJ. Moving beyond the mean in studies of mental chronometry: the power of response time distributional analyses. *Curr Dir Psychol Sci* 20: 160–166, 2011.

Brainard DH. The Psychophysics Toolbox. *Spat Vis* 10: 433–436, 1997.

Britten KH, Shadlen MN, Newsome WT, Movshon JA. The analysis of visual motion: a comparison of neuronal and psychophysical performance. *J Neurosci* 12: 4745–4765, 1992.

Bruine de Bruin W, Parker AM, Fischhoff B. Individual differences in adult decision-making competence. *J Pers Soc Psychol* 92: 938–956, 2007.

Cox RW. AFNI: software for analysis and visualization of functional magnetic resonance neuroimages. *Comput Biomed Res* 29: 162–173, 1996.

Dosenbach NU, Fair DA, Cohen AL, Schlaggar BL, Petersen SE. A dual-networks architecture of top-down control. *Trends Cogn Sci* 12: 99–105, 2008.

Duncan J, Owen AM. Common regions of the human frontal lobe recruited by diverse cognitive demands. *Trends Neurosci* 23: 475–483, 2000.

Eickhoff SB, Paus T, Caspers S, Grosbras MH, Evans AC, Zilles K, Amunts K. Assignment of functional activations to probabilistic cytoarchitectonic areas revisited. *Neuroimage* 36: 511–521, 2007.

Freeman JB, Dale R. Assessing bimodality to detect the presence of a dual cognitive process. *Behav Res Methods* 45: 83–97, 2013.

Fischl B, Salat DH, Busa E, Albert M, Dieterich M, Haselgrove C, van der Kouwe A, Killiany R, Kennedy D, Klaveness S, Montillo A, Makris N, Rosen B, Dale AM. Whole brain segmentation: automated labeling of neuroanatomical structures in the human brain. *Neuron* 33: 341–355, 2002.

Furl N, Averbeck BB. Parietal cortex and insula relate to evidence seeking relevant to reward-related decisions. *J Neurosci* 31: 17572–17582, 2011.

Gao T, McCarthy G, Scholl BJ. The wolfpack effect. Perception of animacy irresistibly influences interactive behavior. *Psychol Sci* 21: 1845–1853, 2010.

Glover GH, Li TQ, Ress D. Image-based method for retrospective correction of physiological motion effects in fMRI: RETROICOR. *Magn Reson Med* 44: 162–167, 2000.

Gold JI, Shadlen MN. The neural basis of decision making. *Annu Rev Neurosci* 30: 535–574, 2007.

Gotts SJ, Simmons WK, Milbury LA, Wallace GL, Cox RW, Martin A. Fractionation of social brain circuits in autism spectrum disorders. *Brain* 135: 2711–2725, 2012.

He BJ, Snyder AZ, Zempel JM, Smyth MD, Raichle ME. Electrophysiological correlates of the brain's intrinsic large-scale functional architecture. *Proc Natl Acad Sci USA* 105: 16039–16044, 2008.

Heekeren HR, Marrett S, Ruff DA, Bandettini PA, Ungerleider LG. Involvement of human left dorsolateral prefrontal cortex in perceptual decision making is independent of response modality. *Proc Natl Acad Sci USA* 103: 10023–10028, 2006.

Honey CJ, Sporns O, Cammoun L, Gigandet X, Thiran JP, Meuli R, Hagmann P. Predicting human resting-state functional connectivity from structural connectivity. *Proc Natl Acad Sci USA* 106: 2035–2040, 2009.

Jo HJ, Saad ZS, Simmons WK, Milbury LA, Cox RW. Mapping sources of correlation in resting state FMRI, with artifact detection and removal. *Neuroimage* 52: 571–582, 2010.

Kayser AS, Buchsbaum BR, Erickson DT, D'Esposito M. The functional anatomy of a perceptual decision in the human brain. *J Neurophysiol* 103: 1179–1194, 2010.

Krishna BS, Ipata AE, Bisley JW, Gottlieb J, Goldberg ME. Extrafoveal preview benefit during free-viewing visual search in the monkey. *J Vis* 14: 6, 2014.

Leopold DA, Maier A. Ongoing physiological processes in the cerebral cortex. *Neuroimage* 62: 2190–2200, 2012.

Lewis CM, Baldassarre A, Committeri G, Romani GL, Corbetta M. Learning sculpts the spontaneous activity of the resting human brain. *Proc Natl Acad Sci USA* 106: 17558–17563, 2009.

Liverant S, Scodel A. Internal and external control as determinants of decision-making under conditions of risk. *Psychol Rep* 7: 59–67, 1960.

Luce RD. *Response Times: Their Role in Inferring Elementary Mental Organization*. New York: Oxford Univ. Press, 1986.

Mennes M, Kelly C, Zuo XN, Di Martino A, Biswal BB, Castellanos FX, Milham MP. Inter-individual differences in resting-state functional connectivity predict task-induced BOLD activity. *Neuroimage* 50: 1690–1701, 2010.

Mennes M, Zuo XN, Kelly C, Di Martino A, Zang YF, Biswal B, Castellanos FX, Milham MP. Linking inter-individual differences in neural activation and behavior to intrinsic brain dynamics. *Neuroimage* 54: 2950–2959, 2011.

Meriau K, Wartenburger I, Kazzer P, Prehn K, Lammers CH, van der Meer E, Villringer A, Heekeren HR. A neural network reflecting individual differences in cognitive processing of emotions during perceptual decision making. *Neuroimage* 33: 1016–1027, 2006.

Nelson SM, Dosenbach NU, Cohen AL, Wheeler ME, Schlaggar BL, Petersen SE. Role of the anterior insula in task-level control and focal attention. *Brain Struct Funct* 214: 669–680, 2010.

Pelli DG. The VideoToolbox software for visual psychophysics: transforming numbers into movies. *Spat Vis* 10: 437–442, 1997.

Ploran EJ, Nelson SM, Velanova K, Donaldson DI, Petersen SE, Wheeler ME. Evidence accumulation and the moment of recognition: dissociating perceptual recognition processes using fMRI. *J Neurosci* 27: 11912–11924, 2007.

Power JD, Barnes KA, Snyder AZ, Schlaggar BL, Petersen SE. Spurious but systematic correlations in functional connectivity MRI networks arise from subject motion. *Neuroimage* 59: 2142–2154, 2012.

Ratcliff R. A theory of memory retrieval. *Psychol Rev* 85: 59–101, 1978.

Ratcliff R, McKoon G. The diffusion decision model: theory and data for two-choice decision tasks. *Neural Comput* 20: 873–922, 2008.

Soane E, Chmiel N. Are risk preferences consistent? The influence of decision domain and personality. *Pers Individ Dif* 38: 1781–1791, 2005.

Stanovich KE, West RF. Individual differences in reasoning: implications for the rationality debate? *Behav Brain Sci* 23: 645–665, 2000.

Treadway MT, Buckholtz JW, Schwartzman AN, Lambert WE, Zald DH. Worth the "EEfRT"? The effort expenditure for rewards task as an objective measure of motivation and anhedonia. *PLoS One* 4: e6598, 2009.